Acta Cryst. (1976). A32, 793

Examination of the Graphite Structure by Convergent-Beam Electron Diffraction

BY P. GOODMAN

Division of Chemical Physics, CSIRO, P.O. Box 160, *Clayton, Victoria, Australia* 3168

(*Received* 1 *March* 1976; *accepted* 5 *April* 1976)

An examination of graphite has been carried out by convergent-beam electron diffraction for the purpose of examining the symmetry of the structure, and of measuring the structure factors for the 100 and the 110 reflexions. Symmetry changes within the sample were related to the fault structure, which was imaged in the defocused convergent beam. The value determined for V_{100} deviates by approximately 9% from the value determined using Dirac–Slater scattering curves for a spherical atom. A difference Fourier map calculated from the experimental values and computed spherical atom values shows the trigonal regions of bonding potential, but lacks resolution, indicating a need to refine other reflexions in the zone.

1. Introduction

Since the derivation of the classical graphite structure by Bernal (1924) there has been almost continuous debate over possible deviations from this structure, prompted by conflicting experimental evidence. Thus, extra reflexions suggesting a larger unit cell were found by electron diffraction (Hoerni & Weigle, 1949), early X-ray evidence calling into question the hexagonal symmetry was summarized by Lukesh (1950), while more recent data encouraged continuation of this debate (Ergun, 1973). Also there were several early reports of an anomalously high ratio for F_{100}/F_{110} which was variously attributed to an alternative structural form (Pauling & Lukesh, 1950) and to bonding effects (Franklin, 1950). Most recently, however, results of a neutron diffraction study were reported in which single crystals of exceptional quality were preselected by X-ray diffraction techniques (Trucano & Chen, 1975). These results confirm the classical structure determined by Bernal, though the authors are careful to point out that their accurate bond measurements are averaged over time and over a large number of unit cells. The present paper reports measurements made at the other extreme, from microscopic crystalline regions, and using very short exposure times of a fraction of a second, by means of convergent-beam electron diffraction. One aim is to show that quite precise symmetry and intensity data can be obtained with this technique from a randomly chosen sample of cleaved graphite, with relatively little time and effort when compared with other techniques requiring larger and more perfect samples. The technique must necessarily be confined to *hk*0 and low-index *hkl* reflexions, and is unsuited to collecting 00*l* data. Working within this limitation, however, we obtain accurate values for the structure factors V_{100} and V_{110} and also resolve other structural points in question.

A new method for analysing convergent-beam data has been introduced in the quantitative section of this work (§§ 3 & 4), partly as a result of working in the particular crystal thickness region of around 40 unit cells, but mainly from the desire to optimize the relevant information content of each *N*-beam calculation (since the method could also be applied in part to crystals of somewhat greater thickness). In this procedure we measure only one point in a convergent-beam diffraction disc accurately, either for angular coordinates of an intensity maximum, or for absolute or relative intensity. The rest of an intensity distribution (in the latter case) is then used simply to define the angular coordinates (*i.e.* the precise incident-beam direction) corresponding to the point, which is carefully chosen to be most sensitive to the parameter in question, *e.g.* structure factor, thickness, *etc.*, and insensitive to other parameters. This method allowed us to develop a more practical and economic working procedure than has previously been reported.

Thin-crystal analysis

While for some time it has been possible to obtain data from regions of 100 Å in cross section (Goodman & Lehmpfuhl, 1965) and thus to extend the scope of precise investigation to specimens of relatively high fault density, only recently have we realized the advantages gained in quantitative structure analysis from the use of very *thin* crystals. Use of the thinnest possible crystals not only removes the influence of absorption to within experimental accuracy, but greatly simplifies the processing of the data. We are finally restricted by the minimum scattering volume consistent with a short exposure time. This limiting volume depends upon the atomic masses in the scatterer. The minimum usable thickness varies from 3 unit cells for MoO_3 to approximately 30 unit cells for graphite, taking into account the practical requirement of a 100 to 200 Å illuminated crystal cross section. The absorption and elastic scattering both decrease as the atomic mass decreases, so that a no-absorption treatment of data can be retained for the light elements (see Goodman & Moodie, 1975).

The equipment used for this investigation was a

Siemens Elmiskop 1 electron microscope which has been modified to permit quantitative convergent-beam measurements (see Dowell, Goodman & Williams, 1976).

2. Symmetry and size of unit cell

Points raised from previous data regarding possible discrepancies from the classical graphite structure may be summarized as follows: (*a*) non-hexagonal symmetry, (*b*) extra reflexions, and (*c*) anomalous values for 100 and 110 structure factors. These points were examined in that order.

A graphite flake was peeled from a block of pyrolytic graphite and placed on a specimen grid. The specimen was used in the back focal plane of the modified Siemens Elmiskop 1. Although the sample had a moderately high fault density and was covered with debris consisting largely of extra flecks of graphite, it was readily possible to focus the electron probe between the debris and faults and determine the crystal symmetry from the [001] zone-axis pattern. A micrograph of the region of crystal used, taken with a defocused convergent beam, appears in Fig. 1, and the zone-axis patterns obtained appear in Fig. 2. Three distinct symmetries were observed: trigonal symmetry (3*m*) was the most common (Fig. 2*a*), but also rectangular symmetry (1*m*) (Fig. 2*b*) and, most rarely, hexagonal symmetry (6*mm*) (Fig. 2*c*) were found. Trigonal symmetry in graphite patterns was analysed by Johnson (1972) and shown to arise from stacking faults. This conclusion agrees with our present observation that symmetry changes occur on crossing dislocation lines. Rectangular symmetry always occurs close to the line of contrast caused by a partial dislocation, and is interpreted by us as being caused by a region in which the Burgers vector displacement is incomplete and unique. This interpretation is supported by the fact that the unique direction in the diffraction pattern is always perpendicular to the dislocation line. This means that the partial dislocation caused by an extra atomic row in a particular layer requires at least 20 or 30 unit cells in which to resolve into a threefold degeneracy. Since the partial dislocations tend to occur in parallel arrays (Fig. 1) it is clear that a wide-area diffraction pattern from this specimen would have an apparent orthorhombic, as well as trigonal, component. This particular crystal is rather heavily dislocated; however, suitable analogous conclusions can be drawn concerning experiments using crystals or crystal regions of lower dislocation density and larger volume.

In further analysis only patterns from hexagonal regions, which are assumed to represent perfect hexagonal graphite, were used. Although it is known that with *N*-beam dynamic diffraction patterns from classically hexagonal graphite will have a small trigonal content (described here in § 6.3), this content is far smaller than that due to a stacking fault in any layer other than a near-surface layer. If there is a fault in a near-surface layer, it is hardly effective in distorting the results. We therefore feel confident in our ability to select regions of effectively perfect *AB* hexagonal stacking.

The next point was to check for extra inner reflexions. For this purpose heavy over-exposures were made from hexagonal regions (see, for example, Fig. 3). However, in no case was any trace found of a twofold superlattice as reported by Hoerni & Weigle (1949), although our method would be capable of detecting reflexions as weak as $\frac{1}{1000}$ of the main reflexion intensities. It was therefore assumed that observations of reflexions of index ($h=\frac{1}{2}$) have been due to double diffraction, faulting, or alternative structures occurring in the particular samples examined.

3. Intensity measurement: general procedure and V_0^i estimate

The actual method of intensity measurement was one involving a combination of photographic densitometry and electronic exposure control, described by Dowell, Goodman & Williams (1976).

The present experimental method for structure-factor determination involves the measurement of the relative intensity of the reflexion concerned (*i.e.* the measurement of the reflexion whose structure-factor is to be determined, relative to the zero beam) at the exact position of zero excitation error, and in the position of symmetrical excitation of the other zone reflexions. The orientation required for this position to be accessible is obtained by turning the crystal away from the zone orientation of Fig. 2(*a*)–(*c*), towards the required reflexion. The point in the intensity disc corresponding to this symmetrical, exact excitation, which also is the point where the intensity has greatest sensitivity to structure factor, may then be located from the symmetry of the surrounding distribution (see Figs. 4 and 5).

We also have access to absolute intensities and so are in a position to measure total absorption. An accurate measurement of V_0^i, the mean coefficient of absorption, appears to be of no particular value, but approximate values are of interest. In general a preliminary measurement of other Fourier coefficients V_h^i is required. However, observations made with single strong reflexions 100, 110, and some higher order reflexions satisfied far from the zone-axis orientation, showed these coefficients V_{100}^i, V_{110}^i, *etc.* to be very small, and less than 0·1 volt. A read-off value from multiple timed exposures was therefore readily obtainable with an accuracy of about 5%.

The crystal was oriented into a near-kinematic orientation such that no close-in reflexions were excited. In this case practically all the reduction in intensity of the direct transmitted beam is due to V_0^i. The measured value (I_0/I_i) of 0·61, where I_0 is the direct transmitted intensity and I_i the incident intensity, yields a value

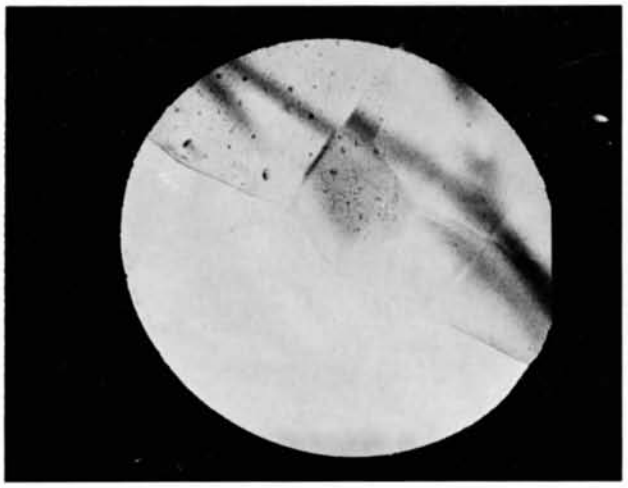

Fig. 1. Micrograph of the region of the graphite flake used in the present investigation. High fault and decoration densities are evident.

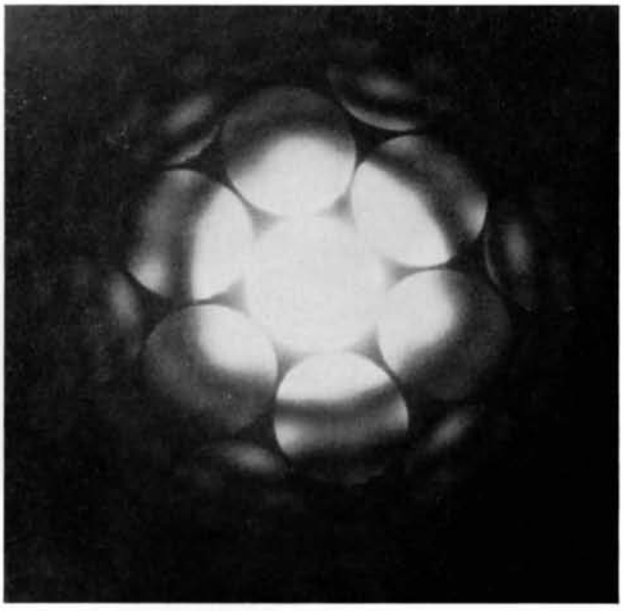

(*a*)

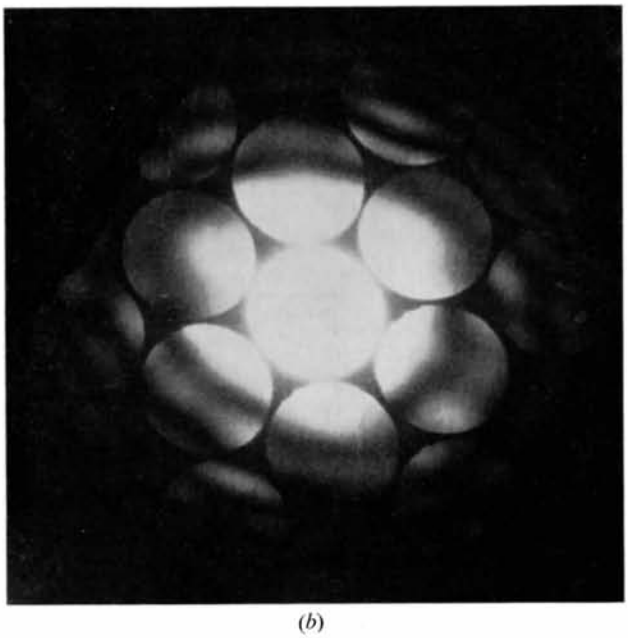

(*b*)

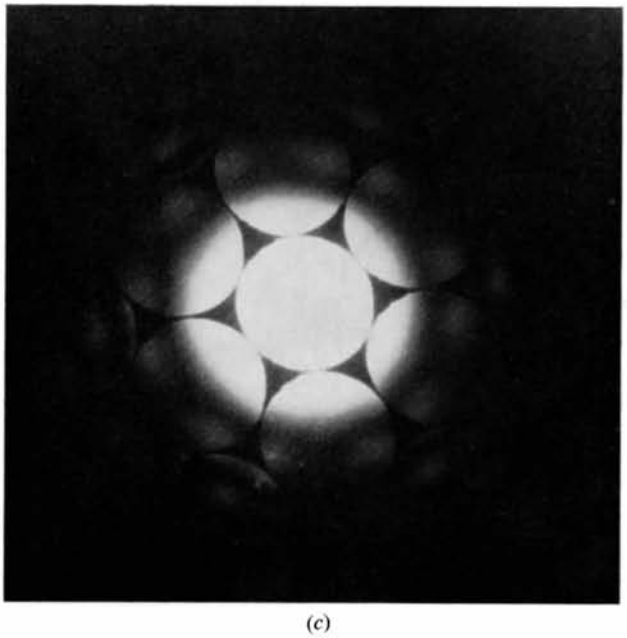

(*c*)

Fig. 2. [001] zone-axis patterns from graphite showing three distinct symmetries. (*a*) Pattern from trigonal graphite occurring because of the presence of a partial dislocation. (*b*) Pattern from orthorhombic graphite which is found close to a fault line of the image (Fig. 1). (*c*) Pattern from hexagonal graphite. The hexagonal region used for this pattern was used for further measurements, including the measurement of structure factors.

[*To face p.* 794

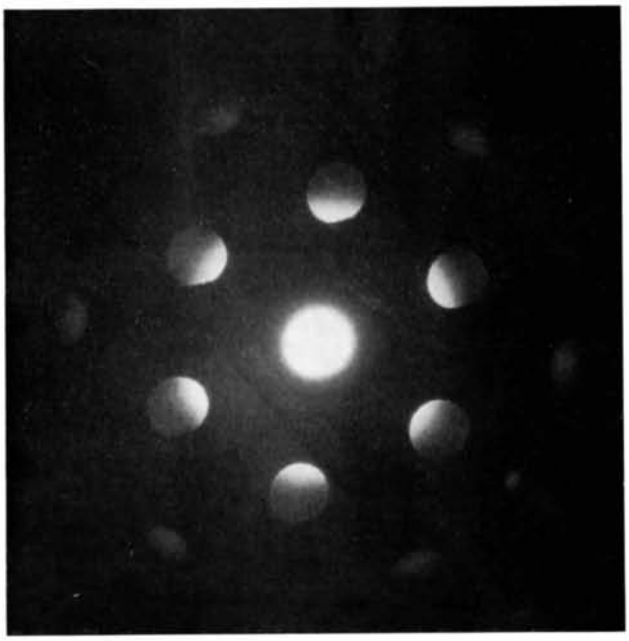

Fig. 3. A moderately exposed zone-axis pattern from the hexagonal region, using a small aperture. Heavy over-exposures of the same pattern were also taken, but no extra reflexions were detected.

Fig. 5. Similar pattern to that of Fig. 4. for the symmetrical excitation of a 110 indexed reflexion.

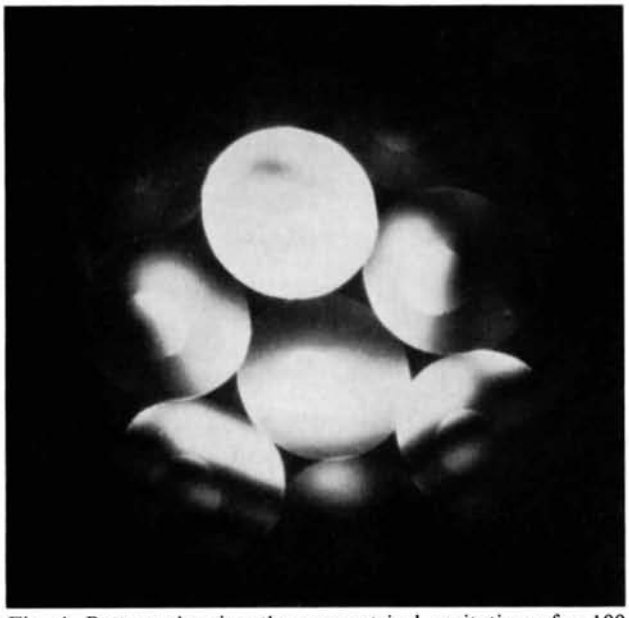

Fig. 4. Pattern showing the symmetrical excitation of a 100 indexed reflexion adjacent to the [001] zone-axis. Both large and small apertures are shown by means of a double exposure.

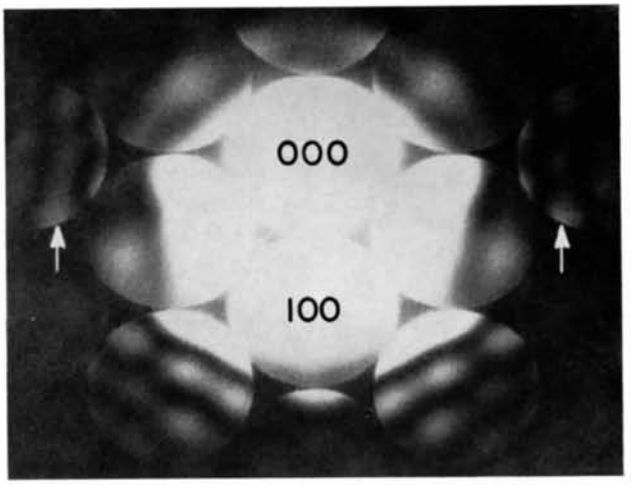

Fig. 9. Convergent-beam exposure at the same setting as in Fig. 4 with the subsidiary maxima of the side beams of index $1\bar{2}10$ and $\bar{1}2\bar{1}0$ indicated by arrows. The positions of these maxima were used to obtain an accurate estimate of the crystal thickness.

for V_0^i of 1·0 volt for a crystal thickness of 270 Å.

It is interesting to compare this value with those for MgO of $V_0^i=0{\cdot}6$ and $V_h^i=0{\cdot}14$ volt (Goodman, 1971). The relatively high value of V_0^i for graphite together with low values for V_h^i fit in with the generally accepted view that the former term arises mostly from plasmon losses, and the latter mostly from thermal diffuse scattering.

4. Relationship between V_{100} and V_{110}

The crystal region found to have accurate hexagonal symmetry from the previous exposures (Fig. 2) was chosen for structure-factor investigation. First the crystal thickness was estimated from a near two-beam excitation of a high-order reflexion, using the separation between subsidiary intensity maxima, and found to be around 270 Å. This estimate was necessarily rough. Then the crystal was returned to the [001] zone-axis setting and tilted further to satisfy one of the 100-indexed reflexions in the symmetrical condition shown in Fig. 4, *i.e.* around the position of equal excitation errors for neighbouring reflexions, so that $\zeta_{10\bar{1}0}=0$, and $\zeta_{1\bar{1}00}=\zeta_{01\bar{1}0}$, using the *hkil* system of indices. After finding the orientation with a large aperture, a small aperture was inserted centrally as indicated in Fig. 4, and then used in a separate exposure. This effectively isolated the angular region required and reduced background to an acceptable level. The background-corrected value of the intensity ratio I_{100}/I_{000} was 1·06. Next, a second orientation was obtained involving the symmetrical excitation of a 110-indexed reflexion as shown in Fig. 5. The same procedure described above was followed. The background-corrected value I_{110}/I_{000} of 1·20 was found from a small-aperture pattern. The method of reading the elastic scattering from the microdensitometer trace is indicated in Fig. 6, and has been described by Goodman (1972).

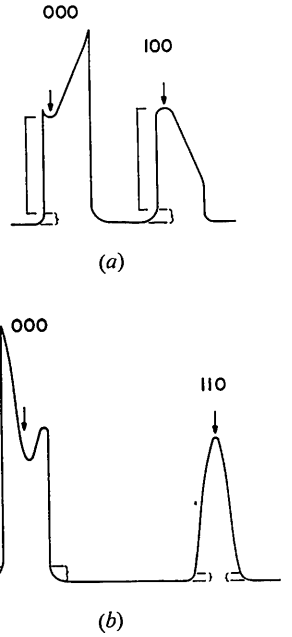

Fig. 6. (*a*) and (*b*) Microdensitometer traces for the patterns shown in Figs. 4 & 5, respectively. The inelastic contribution at the points of zero excitation error is indicated by curly brackets and the elastic contribution by square brackets. The arrows indicate the measured points.

Multislice calculations were made for graphite using 861 beams, at first using a thin-phase grating input based on the projected potential of one unit cell. This was a convenient approximation which was finally checked against the accurate calculation based on the projected potential of each atomic layer. The method of calculation is described in Goodman & Moodie (1974). The first calculations were made using the analytical expression for the atomic scattering factor for neutral carbon derived by Cromer & Waber (1965) from Dirac–Slater (DS) wave functions, together with a temperature factor of $B=0{\cdot}2$. This atomic scattering curve agreed closely with that listed for a neutral unbonded carbon atom in Table 3.3.1*A* of *International Tables for X-ray Crystallography* Vol. III (1962), but diverged significantly from the relativistic Hartree–Fock values tabulated by Doyle & Turner (1967). In what follows, structure factors due to Cromer & Waber will be identified by DS, and those due to Doyle & Turner by R–HF. The R–HF values were not used in our calculations, but values appear for comparison in Table 1. It had been noted that a curve for covalent carbon due to McWeeny (1951) also listed in Table 3.3.1*A* differed only very slightly from that listed for unbonded carbon. On examining the data it was immediately obvious that the DS scattering factors needed more substantial correction since no value of crystal thickness could be found to fit the experimental ratios. To obtain internal consistency both V_{100} and V_{110} needed correcting. Because at this thickness these intensity ratios were close to unity, the direction of correction required was obvious and the amount readily estimated. In particular with the DS spherical atom values, $I_{110}/I_{000}>1$ only for $H>290$ Å; $I_{100}/I_{000}\simeq 1$ only for $H<254$ Å, where H is the crystal thickness. By allowing the parameters V_{100} and V_{110} to be varied in a series of N-beam calculations we were able at this stage to establish a relation between these parameters which was a condition for internal experimental consistency; *i.e.* in order that Figs. 4 and 5 refer to a single crystal thickness. Since the exact thickness was not yet determined, this procedure produced a curve, which is shown in Fig. 7. It was necessary to depress the V_{100} DS value substantially and to raise the V_{110} DS value slightly to follow this curve. The crystal thicknesses to which the calculations correspond are shown in Fig. 7 and in Table 2, and range from 260 to 290 Å, or from 38 to 44 unit cells.

Fig. 8 shows a difference Fourier map obtained by using $V_h(\text{exp})-V_h(\text{DS})$ for a single unit cell in [001]

Table 1. *Comparison of the results obtained by electron diffraction for the structure factors V_{100} and V_{110} with the corresponding values derived from Dirac–Slater (DS) and relativistic Hartree–Fock (R–HF) scattering curves for a spherical atom. The equivalent values for the X-ray scattering factors F_{100} and F_{110} are also shown*

	V_{hkl} (volt)		
Reflexion	R–HF	DS	Values from electron diffraction
100	1·69	1·62	1·45 ± 0·03
110	3·12	3·07	3·15 ± 0·03
	F_{hkl}		
Reflexion	R–HF	DS	Values from electron diffraction
100	3·08	3·19	3·48
110	7·43	7·70	7·27

Table 2. *Calculated points for the curve of Fig. 7, showing the relation between the two structure factor values V_{100} and V_{110} found from the experimental intensities, together with the crystal thicknesses to which each pair of values corresponds*

The row of values arrived at by an independent measurement of crystal thickness is indicated by an arrow. In moving away from the region of the curve corresponding to this crystal region, the difficulty in obtaining agreement between H_{100} and H_{110} also increases, as shown by the values in the last row in the table.

	V_{100} (volt)	V_{110} (volt)	H_{100} (unit cells)	H_{110} (unit cells)
	1·40	3·07 (DS)	44	43
→	1·45	3·15	42	42
	1·50	3·20	40	41
	1·55	3·30	39	40
	1·62 (DS)	3·30	37	42

projection, and using values for V_{100}(exp) and V_{100}(exp) from the central region of the curve of Fig. 7. The trigonal covalent bonding potential is clearly indicated around the single atoms of the projection, marked $C1$ in Fig. 8. Since the Fourier map is for potential rather than charge density the bonding directions show low value contours, and higher-potential regions extend in the non-bonding directions. This Fourier map also clearly indicates the need for other structure factors to be refined in order to obtain more detail in the bonding distribution.

5. Determination of thickness and of V_{100} and V_{110}

An exact determination of the crystal thickness at this stage would allow a precise determination of the two structure factors to be made. Although a large region of the curve of Fig. 7 could be excluded on the grounds of yielding unrealistic structure-factor corrections, such subjective decisions would not then be required. It has been well known for some time that weak-beam intensity modulations can be used to determine crystal thickness numerically. However, earlier methods (Goodman & Lehmpfuhl, 1967) required calculation of a whole rocking curve, over a limited range, with consequent computational expense and labour which would become a real limitation when, as in the present case, two-dimensional interactions between several hundreds of beams need to be included. Recent experience in determining the thickness of very thin MoO_3 crystals (Dowell, Goodman & Tate, 1976) by comparing intensity measurements with calculations for one setting encouraged the search for a similar method here. With very thin crystals (say 1–6 unit cells), there is no intensity modulation within the convergent-beam discs; furthermore the stepwise increase of diffracted intensity with layer-by-layer increase in thickness is readily detectable. Since the pattern from a crystal of thickness 40 unit cells no longer has this simple character, a different procedure, depending upon locating a turning point rather than measuring an intensity value, had to be adopted in the present case to determine the thickness to within the required

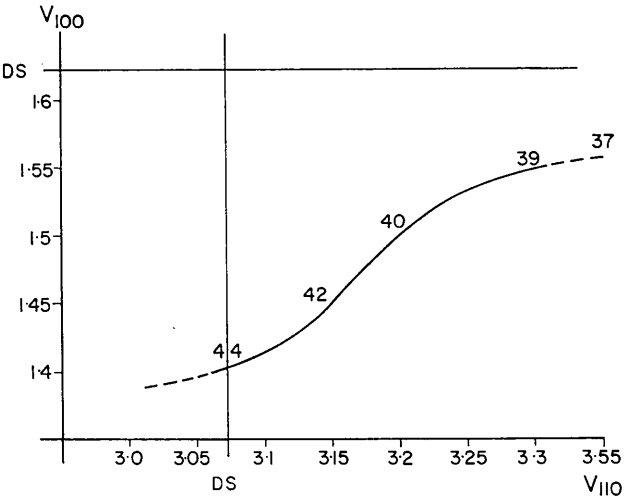

Fig. 7. A curve showing the relation required between values for the structure factors V_{100} and V_{110} for internal experimental consistency. The numbers placed along the curve indicate the crystal thicknesses in unit cells to which points on the curve correspond. DS indicates a Dirac–Slater value.

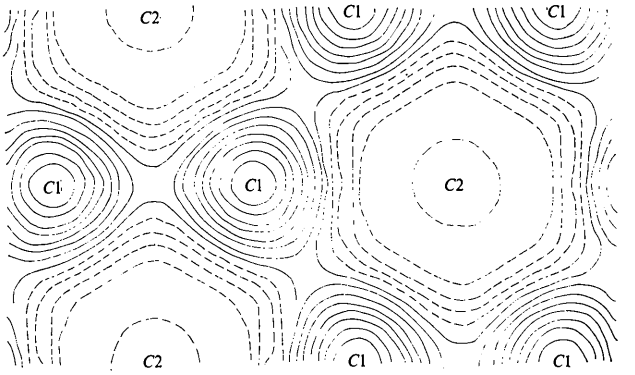

Fig. 8. A difference Fourier map of the [001] projection, using the experimentally determined and the theoretical DS structure factors.

accuracy of one unit cell. Firstly, using a large-aperture pattern in which the 100 reflexion was symmetrically excited, the angular coordinates of the subsidiary maxima in the weakly excited $\bar{1}\bar{1}0$ side beams were measured (actual indices $1\bar{2}10$, $\bar{1}2\bar{1}0$, for the $10\bar{1}0$ pattern; see Fig. 9). Then the N-beam calculation corresponding to this angle of incidence was run, and the position of the local intensity maximum in the intensity *vs* thickness curve of the $\bar{1}\bar{1}0$ beams gave an accurate thickness value. This procedure depends upon the fact that a local intensity maximum in the rocking curve (intensity *vs* angle) corresponds to a local maximum in the intensity *vs* thickness curve calculated for that angle. The thickness determination was independent of the values of structure factors within the range of the refinement used in this calculation. This relative independence arises because the weak beam was measured at a substantial excitation error.

From a measurement of the subsidiary $\bar{1}\bar{1}0$ fringes indicated in Fig. 9, a thickness value of between 41 and 42 unit cells, or $41\frac{1}{2}\pm\frac{1}{2}$ unit cells, was obtained. This gives values from the curve of Fig. 7 of $V_{100}=1{\cdot}45\pm0{\cdot}02$ and $V_{110}=3{\cdot}15\pm0{\cdot}03$ volt. The experimental error is allocated by considering the uncertainty in crystal thickness of one unit cell in selecting the region of the curve of Fig. 7, and other sources of experimental error detailed below. The experimentally determined values are given in Table 1, together with those derived for a spherically symmetric atom. Both DS and R–HF theoretical values are listed. DS values give closer agreement for V_{100}, but no significance is attached to this in view of the apparent importance of bonding effects.

6. Possible sources of error

6.1. *Inelastic background*

Since our calculations refer only to elastic scattering there is always a finite error due to inelastic background which will usually place a final limit on accuracy. We therefore aim firstly to minimize this contribution and secondly to estimate it. This is done by choosing the smallest practical Kossel–Möllenstedt aperture for the pattern used for final measurement, and by estimating the inelastic scattering intensity at the edges of the sharp aperture. This problem and procedure have been described earlier (Goodman, 1972). The final error in intensity measurement from this source can then be estimated.

Since the background measurement is strictly relevant to the intensity just inside the aperture edge, the most reliable estimates of elastically scattered intensity are obtained by arranging that the measured point lies close to an edge. Fig. 6 shows that this has been managed better for the 100 peak than for the 110 peak which is almost central in the aperture. This has caused the uncertainty in I_{110}/I_{000} to be about 5%, actually 1·16–1·22, or about five times greater than the uncertainty in I_{100}/I_{000}. However, the estimated V_h are not linearly related to these ratios: the multislice calculations described below show that a 7·4% reduction in V_{100} leads to a 25% reduction in I_{100}/I_{000}, and that a 4% increase in V_{110} leads to a 30% increase in I_{110}/I_{000}. This favourable situation, reducing the sensitivity of the final results to errors in the estimated intensity ratio, arises from the particular choice of crystal thickness and means that, in this experiment, background was not an important source of error.

6.2. *Errors in outer-reflexion structure factors and temperature factor*

As has been noted above, other structure factors besides V_{100} and V_{110} need refining, notably V_{200} and V_{210}, and to a lesser extent those of the further-out reflexions. Errors in these other parameters, which must be included in our N-beam calculations, will lead to errors in the calculated values for the 100 and 110 reflexions. However, it was found by calculation that, owing to the particular orientations used (symmetrical orientation with the particular reflexion satisfied), the results were insensitive to reasonable variations in these parameters. For example, a 5% depression in V_{200} led to a 2% change in the calculated value of I_{100}/I_{000} in the region of the calculation used in the refinement, and this led to a change of less than 1% in the V_{100} estimate. The error introduced into the V_{110} estimate by similar changes was much less than that for the V_{100} estimate and could be neglected. Furthermore, with such a low temperature factor as $B=0{\cdot}2$, the B factor can be varied quite widely without appreciable influence on the 100 and 110 intensities.

6.3. *Check of numerical results using a single-layer calculation*

By using 861-beam calculations errors arising from omission of zero-layer interactions were eliminated. However, calculations made using the projected potential of a single unit cell as the basis for the input phase-grating amplitudes are of limited accuracy since they omit part of the upper-layer interactions. This problem was discussed by Goodman & Moodie (1974). On the other hand, calculations made for the layered structure of graphite using single atomic-layer projected potentials as a basis for the input phase-grating amplitudes are of very high accuracy, and provide a suitable standard with which to compare other calculations and for final comparison with experiment.

The most significant difference between the single-layer accurate calculation and the single unit-cell calculation referred to is that the accurate calculation reveals the trigonal nature of the pattern obtained from graphite with hexagonal AB stacking. A calculation made for the [001] zone-axis setting using this single-layer calculation shows that the trigonality, expressed as an intensity ratio between two neighbouring 100 indexed reflexions, is an oscillating function of thickness with a periodicity of one unit cell. It is important to realize that although trigonality is great-

est when the thickness is $(n+\frac{1}{2})$ unit cells it is also appreciable at thicknesses corresponding to an integral number of unit cells. Although as a percentage effect it decreases with increasing thickness it is still oscillating between 5 and 10% at around 400 Å thickness. However, trigonality is a maximum at the exact zone axis where the diffracted beams are very weak, and is much less marked when alternative 100 indexed reflexions are satisfied. The weakness of the diffracted beams at the zone-axis setting makes this trigonality just detectable with careful observation, so that there is no difficulty in distinguishing hexagonal crystal regions, from regions containing one or more stacking faults which lead to the strong trigonality shown in Fig. 2.

Comparison of results from the two calculations shows that the single-layer calculation was not necessary for the present determination of structure factors although this could not be known beforehand. Therefore, the key calculations were run again using the single-layer projection approximation. The only significant influence on the results in Table 2 (§ 4) was the reduction of the fitted thickness (the entries in columns 3 and 4) by half a unit cell. The independent calculation (§ 5) to find the turning-point, however, gave the same result (*i.e.* $H=41\frac{1}{2}$ unit cells) as previously: the turning-point calculation is insensitive to the particular approximation used because it corresponds to a high excitation error. Therefore the net result of using the single-layer calculation was actually an improved agreement with the fitted thickness for the row of structure factors indicated by the arrow in Table 2, but this improvement is within our experimental error. However, the single-layer results would be useful both for the observation of half unit-cell surface steps, and for further and more accurate structure refinement.

6.4. *Summary of errors*

In summarizing the sources of error in the present measurements, it has been found that the experimental error comes mainly from the uncertainty in the crystal thickness, an uncertainty which is no greater than one unit cell, and to a lesser extent from the error in measurement of the intensity ratios I_{100}/I_{000} and I_{110}/I_{000} from the microdensitometer curves. This latter error arises from experimental noise and from the need to allow for the inelastic background. In addition possible errors in outer reflexion structure factors increase the uncertainty in the V_{100} estimate by an amount less than 1%. Errors from all other sources appear to be unimportant.

7. Conclusions

This study shows that the classical hexagonal Bernal structure applies to unfaulted and unstrained regions of graphite; other symmetries present in strained regions emphasize the difficulties in obtaining good data by X-ray diffraction, which requires larger crystals. The existence of an 'anomaly' in the structure factor ratio V_{100}/V_{110} (reported in previous X-ray analyses) is confirmed and is shown to be consistent with covalent bonding. The fact that the possible error in the V_{100} determination ($1{\cdot}45 \pm 0{\cdot}03$) is about 2% from the single measurement reported in this paper does not reflect an inherent accuracy limit. Better accuracy could be obtained by accumulating a number of such measurements, in which case accuracies of $<1\%$ should be readily obtainable with this structure.

In conclusion we believe that where the thin-crystal method is applicable it leads to a very rapid interpretation of results. The time involved in an analysis is an important consideration. Whereas in previous types of analysis periods of several months or even longer have been involved, the present analysis – which includes data-collection, analysis, and computer programming and computing – required six weeks. With the method now developed analysis time could be considerably shortened.

Helpful consultations with Drs S. L. Mair and S. W. Wilkins are gratefully acknowledged.

References

BERNAL, J. D. (1924). *Proc. Roy. Soc.* A**106**, 749–773.

CROMER, D. T. & WABER, J. T. (1965). *Acta Cryst.* **18**, 104–109.

DOWELL, W. C. T., GOODMAN, P. & TATE, N. (1976). To be published.

DOWELL, W. C. T., GOODMAN, P. & WILLIAMS, D. (1976). To be published.

DOYLE, P. A. & TURNER, D. S. (1967). *Acta Cryst.* A**24**, 390–397.

ERGUN, S. (1973). *Nat. Phys. Sci.* **241**, 65–67.

FRANKLIN, R. E. (1950). *Nature*, **165**, 71–72.

GOODMAN, P. (1971). *Acta Cryst.* A**27**, 140–147.

GOODMAN, P. (1972). *Acta Cryst.* A**28**, 92–93.

GOODMAN, P. & LEHMPFUHL, G. (1965). *Z. Naturforsch.* **20a**, 110–114.

GOODMAN, P. & LEHMPFUHL, G. (1967). *Acta Cryst.* **22**, 14–24.

GOODMAN, P. & MOODIE, A. F. (1974). *Acta Cryst.* A**30**, 280–290.

GOODMAN, P. & MOODIE, A. F. (1975). Proc. EMAG 75 Meet., Bristol, U.K.

HOERNI, J. & WEIGLE, J. (1949). *Nature, Lond.* **164**, 1088.

International Tables for X-ray Crystallography (1962). Vol. III. Birmingham: Kynoch Press.

JOHNSON, A. W. S. (1972). *Acta Cryst.* A**24**, 534–543.

LUKESH, J. S. (1950). *Phys. Rev.* **80**, 226–229.

MCWEENY, R. (1951). *Acta Cryst.* **4**, 513–519.

PAULING, L. & LUKESH, J. S. (1950). *Amer. Min.* **35**, 125.

TRUCANO, P. & CHEN, R. (1975). *Nature*, **258**, 136–137.